IET Computer Vision

Research Article

IET Journals
The Institution of Engineering and Technology

Set of bilateral and radial symmetry shape descriptor based on contour information

ISSN 1751-9632
Received on 29th October 2015
Revised 23rd November 2016
Accepted on 24th November 2016
E-First on 24th February 2017
doi: 10.1049/iet-cvi.2015.0413
www.ietdl.org

Natalia V. Revollo[1,2] ✉, Claudio A. Delrieux[1], Rolando González-José[3]

[1]*Instituto de Investigaciones en Ingeniería Eléctrica, UNS-CONICET, Avda. Alem 1253, Bahía Blanca, Argentina*

[2]*Facultad de Ingeniería, UNJu, Gorriti 237, Jujuy, Argentina*

[3]*Instituto Patagónico de Ciencias Sociales y Humanas. Centro Nacional Patagónico, CONICET, Bvd. Brown 2915, U9120ACD, Puerto Madryn, Chubut, Argentina*

✉ *E-mail: nrevollo@criba.edu.ar*

Abstract: Form and shape descriptors are among the most useful features for object identification and recognition. Even though there exists a widely used set of shape descriptors and underlying computational methods for their evaluation, frequently they fail to distinguish among very similar objects that they appear very different to the human eye. The authors propose a new set of shape descriptors based on a finer determination of the object symmetry axes, and a more accurate estimation of the bilateral and radial symmetries. These descriptors were thoroughly tested using several synthetic and real objects with varying degrees of symmetry. The methods for axes estimation and symmetry descriptors extraction outperform the widespread shape descriptors in recognising and identifying among very similar objects.

1 Introduction

Shape is likely to be the most important feature for recognising objects in the real word. However, our everyday vocabulary usually lacks adequate words for shape description. In computer vision, shape descriptors are among the most useful features in object recognition and identification, being frequently used in manual or automated classification, recognition or matching in many computer applications [1–4].

In two-dimensional images, the shape of a particular object consists of a group of adjacent pixels segmented together according to some specific criterion, for instance luminance, colour or texture. The widespread approach for shape description is to evaluate a usually small set of features such as form factor, roundness, elongation, and curl among others. However, either by themselves or combined, they are usually not enough to distinguish among objects that look very different to the human eye [1].

There are basically two different feature extraction approaches [5–7], namely, the contour-based, and the whole pixel-set approach. Contour-based methods are the most frequently used since they are simpler and perform with less computational cost [8], being form factor probably the most simple and widely used [1]. In [9], the authors present the evaluation of efficiency for object identification of five simple descriptors: convexity, principal axis ratio, compactness, circular and elliptic variance. These descriptors are suitable to characterise some specific object, i.e. they are useful for some particular geometric figures, like circles or ellipses. This characterisation also includes descriptors of elongation, aspect ratio, solidity among others.

Fourier descriptors are a powerful description method if the forms are single closed curves with moderate polynomial degree [10–13] and therefore different adaptations of the method for character recognition could be found in the literature, such as UNL Fourier features [14]. Contour-based methods also include curvature scale space, chain code, polygon and spline approximations, boundary decomposition and elastic matching [15–19].

On the other hand, region-based methods consider the whole set of pixels of the objects. Most of them are related to moment analysis [20–25] which are mathematically concise, but difficult to correlate with shape features, local features and human visual perception. A small group of region-based descriptors is related to morphology description and shape decomposition [1]. Here, the disadvantage appears when a shape is complex, requiring large number of simple components is needed.

In most classification and recognition applications, several shape descriptors are combined together in a feature vector [4, 8, 26]. To work effectively, these feature vectors are expected to be robust under homographies and luminance changes.

Humans possess a natural visual perception mechanism specifically sensitive to symmetry detection [27, 28]. Increasing evidence indicates that symmetry detection has large potential for computer vision applications [29, 30]. For centuries, *symmetry* has been the subject of study for philosophers, astronomers, mathematicians, artists, architects, and physicists [31].

In nature, symmetry is the result of an equilibrated distribution of shape, being bilateral and radial the most common. The body structure of different organisms exhibits many different configurations presenting bilateral or radial symmetry. Bilateral symmetry is defined through a central axis that divides the object in two equivalent, right and left halves by only one plane. However, some human attributes such as the facial shape possess some degree of asymmetry in normal, non-clinical populations, hinting that perfect symmetry is a theoretical condition rather than a natural condition [32]. Radially symmetric objects resemble a pie where several cutting planes produce roughly identical pieces [33, 34].

The aim of this work is to propose new definitions of bilateral and radial symmetry shape descriptors and to assess their use to classify synthetic and real images. Our main interest is to compute symmetry relationships between areas and perimeters based the location of the main and secondary symmetry axes. In addition, we propose quantification means to evaluate bilateral and radial symmetry measures derived from the area and perimeter distribution. These descriptors can be applied for automatic shape recognition and classification.

2 Methodology

2.1 Main axis determination

Bilateral symmetry occurs if the object is invariant under a reflection about a line (axis of symmetry) passing through the centroid of the object [35]. The main axis can be defined as the line

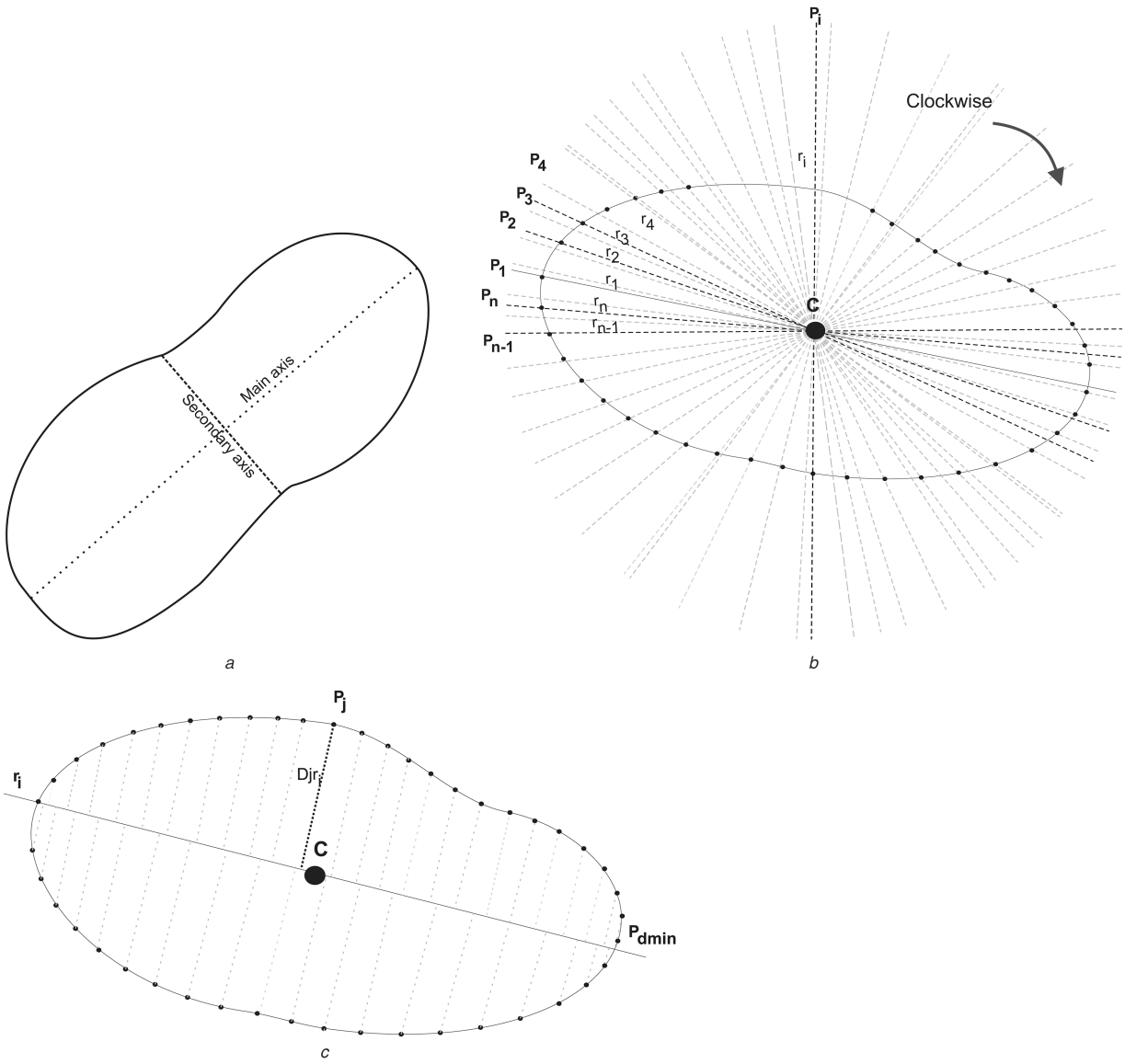

Fig. 1 *Symmetry of an object*

(a) Main and secondary axes of symmetry, ***(b)*** Generation of straight lines between contour point and shape centroid. The lines are computed for all boundary points and the initial point of the sequence is noted as P_1, ***(c)*** Examples of distances from contour points P_j to the line r_i including P_i and C. The pair of opposite points (P_i, $P_{d\min}$) is formed when D_{jr_i} is minimal

with the longest distance passing through the centroid, between any two points on the contour. Also, a secondary axis is considered to calculate radial symmetry. The secondary axis is perpendicular to the main and passes through the centroid (Fig. 1*a*).

The shape is represented by its boundary points without taking into account gap or holes inside the object. Then the contour is represented by a sequence of points: $\boldsymbol{P} = \{P_1, P_2, \ldots, P_n\}$, arranged clockwise. Each element P_i contains the coordinates P_{i_x} and P_{i_y} from the pixels on the image. First, the method determines the shape centroid C as

$$C = (C_x, C_y) \quad \text{with} \quad C_x = \frac{1}{n}\sum_{i=1}^{n} P_x \quad \text{and} \quad C_y = \frac{1}{n}\sum_{i=1}^{n} P_y. \quad (1)$$

The idea behind the algorithm is to find each pair of opposite points located on a line through the centroid and to select those having the largest distance (Fig. 1*b*). For each point P_i the following equations are computed:

$$r_i = y = mx + b, \quad m = \frac{P_{i_y} - C_y}{P_{i_x} - C_x}, \quad b = \frac{P_{i_y} - C_y}{P_{i_x} - C_x}(-P_{i_x}) + P_{i_y}, \quad (2)$$

where m is the slope of the line r_i, b is the y-intercept of the line and x is the independent variable of the function $y = f(x)$. In order to find the opposite point for P_i, the method calculates the distance between each contour points $P_j \neq P_i$ and the straight line established by the previous equation. The distance is obtained from

$$D_{jr_i} = \frac{\left|mPx_j - Py_j + b\right|}{\sqrt{m^2 + 1}}. \quad (3)$$

The minimal value of D_{jr_i} for each P_i is a selected point $P_{d\min}$ which is the nearest point from the contour to the line (Fig. 1*c*). A constraint $|i - j| > k$, with $k > 2$ is defined aiming to avoid the selection of adjacent points. Therefore, the pair (P_i, $P_{d\min}$) is formed and the corresponding axis length L_i result in

$$L_i = \sqrt{(P_{i_x} - P_{d\min_x})^2 + (P_{i_y} - P_{d\min_y})^2}. \quad (4)$$

Finally, the maximum of L_i (here noted as $L_{\max}$) is calculated for the contour. The points P_j and $P_{d\min}$ of maximum length $L_{\max}$ define the location of the main axis of symmetry. Fig. 2 shows some iterations of the algorithm for a given shape.

2.2 Determination of the main and secondary axes of symmetry in a discrete space

The estimated location of the main symmetry axis can be away from the actual axis due to the absence of shape curvature as a result of spatial quantisation (i.e. rasterisation). Therefore, the main axis estimation can be improved taking into account straight segments over the contour (Fig. 3).

The main axis estimation follows three steps: (i) chain coding, (ii) direction coding, and (iii) main axis length estimation. First, the contour is described as a chain code of eight directions based on the subsequent points of the boundary (Fig. 4*a*) and is represented as $\mathbf{CC} = \{\mathrm{CC}_1, \mathrm{CC}_2, \ldots, \mathrm{CC}_n\}$. Second, chain code values at positions i and $i+1$ are used for direction coding. Thus, the method assigns the following:

$$\mathrm{CD}_i = \begin{cases} 1 & \text{if} \quad \mathrm{CC}_i = \mathrm{CC}_{i+1} \\ 0 & \text{otherwise} \end{cases} \quad (5)$$

This codification provides information about the changes of direction corresponding to straight segments in the contour. This implies that the direction code is 1 if the points $P_i - 1$, P_i, and $P_i + 1$ are aligned (Fig. 4*b*). The third step computes an accurate estimation of the length of the main axis. To compensate the distortion in curvature due to spatial quantisation, the method evaluates the neighbour pixels on the boundary with information of the direction encoding. Starting with the pixels (P_a, P_b) that define the estimated main axis, if either of P_a or P_b are placed on a straight segment, the algorithm computes new values for P'_a and P'_b as the average of the pixels in that segment. Finally, the secondary axis is computed as the straight line perpendicular to the main axis (Fig. 5*a*).

2.3 Symmetry descriptors

The new proposed descriptors are estimated after finding the main and secondary symmetry axes. For this purpose, four contour points P_a, P_b, P_c, P_d, and the centroid C are considered, where pairs (P_a, P_b) and (P_c, P_d) correspond to the main and secondary axes, respectively (Fig. 5*b*). In consequence, the shape is subdivided into four regions. For each region, the area A_i and perimeter $\overline{P_i}$ are calculated; e.g. A_4 is the area of the region established within the boundary of points P_a, P_d, and C, while $\overline{P_4}$ is the contour length between these points. Therefore, four descriptors of bilateral symmetry are computed considering the similitude of areas and perimeters. In particular

$$SA_m = \frac{A_1 + A_2}{A_3 + A_4}, \quad SP_m = \frac{\overline{P_1} + \overline{P_2}}{\overline{P_3} + \overline{P_4}}, \quad (6)$$

$$SA_s = \frac{A_1 + A_4}{A_2 + A_3}, \quad SP_s = \frac{\overline{P_1} + \overline{P_4}}{\overline{P_2} + \overline{P_3}}, \quad (7)$$

where SA_m and SP_m are bilateral symmetry descriptors of area and perimeter with respect to the main axis, while SA_s and SP_s are bilateral symmetry descriptors of area and perimeter using the secondary symmetry axis.

Similarly, radial symmetry quantification is addressed from combinations of areas and perimeters. Thus, based on the relationship between the *i*th and *j*th regions, the descriptors are

$$SA_{i,j} = \frac{A_i}{A_j}, \quad SP_{i,j} = \frac{\overline{P_i}}{\overline{P_j}}, \quad i: 1, \ldots, 3, \quad j: i+1, \ldots, 4, \quad (8)$$

Once all possible combinations are obtained, these values are used for the descriptors estimation based on statistic features of the relationship between areas and perimeters. The definition of each radial descriptor is summarised in Table 1.

2.4 Special considerations

The applicability of the proposed descriptors is tied to the quality of the border segmentation. General purpose binarisation methods like Otsu's [36], or even simple thresholding (see the following section) appear to work well. However, occlusion and self-occlusion would affect the assessment of the descriptors. A proper analysis would be done in future works. The geometric basis of the procedure to find the symmetry axes uses only affine operations. Therefore, the proposed shape descriptors are intrinsically invariant under affine transformations (in an ideally continuous space). However, coarse discretisation may be an issue and therefore scale symmetry may break for small scales.

3 Results and discussion

3.1 Synthetic images

As an initial test set, synthetic images on different resolution were used for the determination and validation of symmetry axes. The set of shapes presented in Fig. 6 shows a symmetry degradation from left to right. In addition, these shapes retain similar axes location in order to facilitate the comparison of the results. The disparity between the estimated main axis length and the theoretical one is closed to 2% for the lowest image resolution (Fig. 7*a*), and below 1% for the highest ones (Fig. 7*b*). The results shown in Fig. 6 correspond to the location of the estimated main and secondary axes.

Subsequently, the five shapes proposed in Fig. 6 were scaled and rotated in Fig. 8 with two purposes: (i) to calculate symmetry shape descriptors and (ii) to test their robustness to scaling and rotations. Five particular shapes were included to evaluate the descriptors in the last row of Fig. 8. Table 2 lists the symmetry descriptors to be compared for each shape.

In Fig. 9, the descriptors of SA_m, SA_s, SP_m, SP_s, μ_a, and μ_b were compared to the first 15 shapes of Fig. 8. The low variation observed in the descriptors estimated for each figure (original, rotated, and scaled) could be attributed to the boundary. It is worth noting that the sensitivity is higher to angle variations than scaling variations in most of the cases (Figs. 9*b* and *e*). Nevertheless, descriptors computed for the rotated shape remain highly consistent with the ones computed for the original shapes.

Also, the symmetry level from shapes 1 to 5 is visible in Fig. 9. Despite the differences among the descriptors, it can be noted that the highest values of the descriptors correspond to shape 1, while the lowest values are from shapes 3 to 5. Based on Fig. 8, the less symmetric shape is the fifth. However, shape 3 has less symmetry with respect to the secondary axis, which is correctly estimated by the corresponding descriptor in Fig. 9*b*. Excluding this descriptor, the overall analysis shows the least symmetry for shape 5.

The last group of shapes (16–20) in Fig. 8 was included to assess the application of the algorithm to particular cases. For instance, in shape 16 (a rectangle), the main axis obtained with our method differs from the diagonal. This could reside in the high sensibility of the adjustment algorithm to recognise straight segments over the contour. Another particular case is shape 17, in which the interpretation of the symmetry based on the descriptors could be inconsistent (Table 2). On the one hand, based on the area descriptors, the shape seems to be more symmetric with respect to the main axis ($SA_m = 0.975 > SA_s = 0.88$). On the other hand, the shape results more symmetric with respect to the secondary axis ($SP_m = 0.904 < SP_s = 0.98$). Nevertheless, the shape results highly symmetric when all the descriptors (Table 2) are considered in the analysis. This example demonstrates ability the proposed symmetry descriptors to evaluate radial symmetry. Specifically,

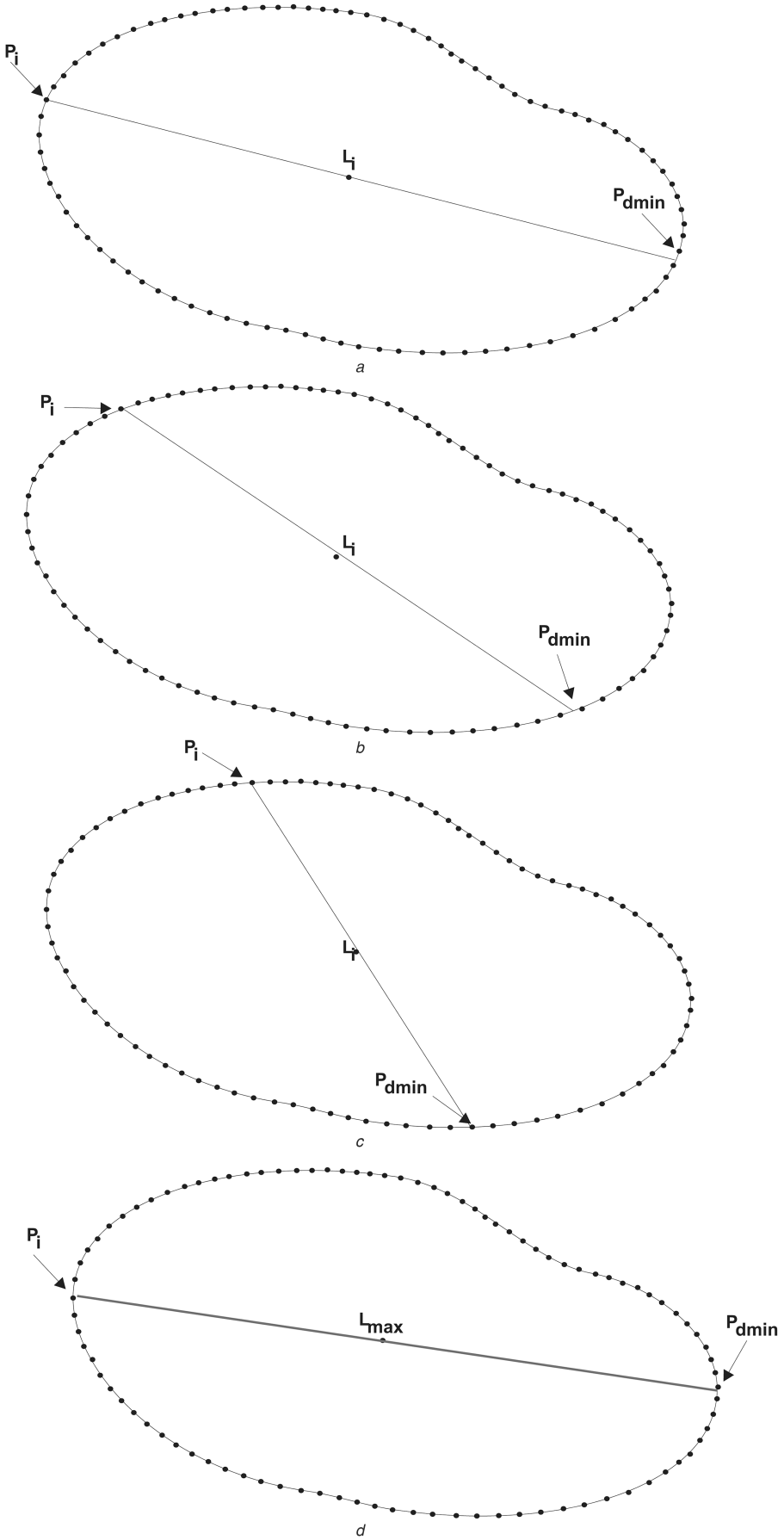

Fig. 2 *Three steps of the iterative computing of axis length (a), (b), and (c). The algorithm finds the maximum length L_{max} to establish the main axis*

this shape can be classified as 'moderate radially symmetric' with respect to the considered axes, but the addition of more axes to analyse may improve the symmetry evaluation. It is worth noting that the algorithm proposed uses the centroid instead of the midpoint as shown in shape 18 – a triangle –.

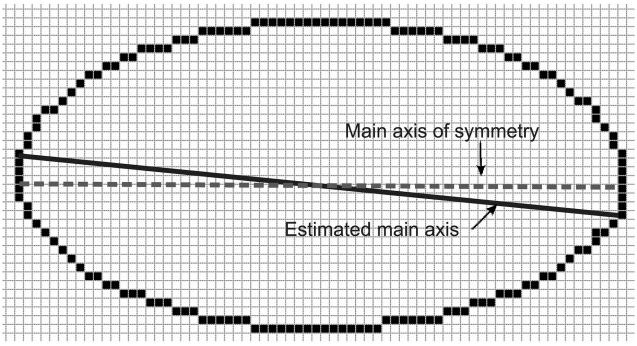

Fig. 3 *Estimated main axis and the main symmetry axis differ due to spatial quantisation*

The fourth special case, shape 19, corresponds to a shape with a marked unbalanced symmetry. For this case, the perimeter descriptors (Table 2) appear to be consistent with a symmetric shape ($SP_m > 0.9$ and $SP_s > 0.98$), whereas only (SA_s=0.68) indicates asymmetry. Concerning the discrepancy between these descriptions, the use of the radial statistic ones becomes more convenient to analyse symmetry. For instance, the asymmetry of shape 19 is revealed by the high standard deviation ($\sigma_A = 0.151$, $\sigma_P = 0.114$) and the high difference between maximum ($Max_A = 1$, $Max_P = 0.988$) and minimum ($Min_A = 0.61$, $Min_P = 0.834$) of area and perimeter, respectively. The final conclusion is that shape 19 is 'poorly radially symmetric'.

Finally, shape 20 is a 'five corner' object in which the radial symmetry cannot be defined by two perpendicular axes. These can be observed in Table 2 where the first four descriptors describe a wide variation. In addition, the other statistic descriptors confirm the asymmetry and thus we classified this figure as 'very poorly radially symmetric'.

3.2 Real images

Symmetry descriptors were also evaluated in the context of Biology images. The sample is a set of diatoms images extracted from Automatic Diatom Identification and Classification (ADIAC) image database [http://www.ualg.pt/adiac/pubdat/pubdat.html, ADIAC, CEC contract MAS3-CT97-0122.]. The ADIAC project works in the continuous developing of algorithms for automatic recognition and classification of diatoms using digital image processing [http://rbg-web2.rbge.org.uk/ADIAC/adiac.html]. The greatest proportion of the diatom genera is bilaterally symmetrical about two orthogonal axes. A much smaller number of the genera are bilaterally symmetrical about only one axis and also some genera are rotationally symmetrical.

First, the grey level diatoms images were binarised using a simple thresholding method (see Fig. 10*a*). After segmentation, the contours were extracted and the symmetry descriptors were

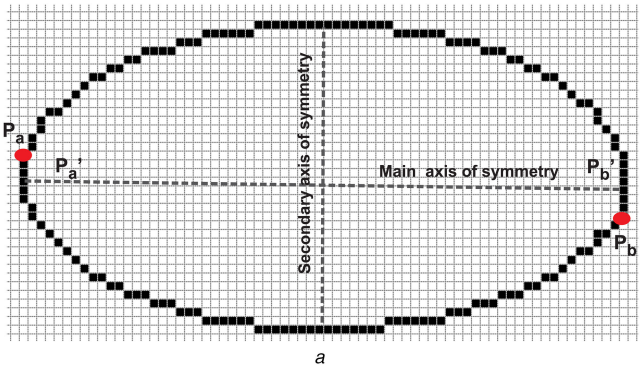

a

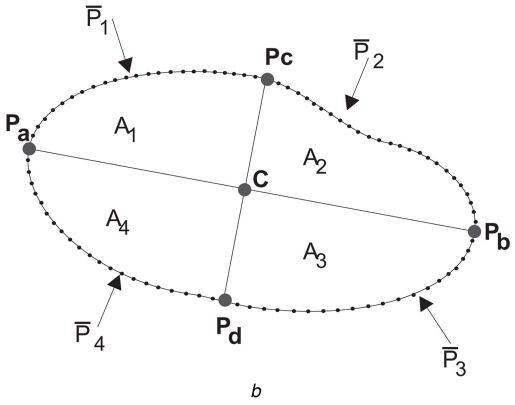

b

Fig. 5 *Symmetry axes improvement and region selection*
(a) Main symmetry axis after improvement, and the secondary axis, ***(b)*** Shape division into four regions. Areas A_i and perimeters $\overline{P_i}$ are used to compute the symmetry descriptors

estimated. Fig. 10*b* shows the full set of diatoms with the detected contours superimposed. Table 3 summarises the corresponding descriptors for each shape.

Considering the SA_m descriptor, the highest values correspond to shapes 7, 2, 8, and 11 ($SA_m > 0.99$) while the lowest value is for shape 17 ($SA_m = 0.779$), which is consistent with a visual analysis of these shapes. Then, a detailed inspection of shapes 7 and 8 reveals its low symmetry with respect to the secondary axis ($SA_s = 0.705$), in contrast with shape 17 that now presents a higher value ($SA_s = 0.959$). Also the most symmetrical shapes referred to the secondary axis are 5, 6, 10, 11, and 18 ($SA_s > 0.98$). If we perform an analysis with respect to both axes simultaneously, we can distinguish shape 11 as the most symmetric. However, this analysis does not allow to recognise the less symmetric shape.

Regarding the perimeter descriptors, the less symmetrical shapes are 4 and 6 with respect to the main axis ($SP_m < 0.84$) and

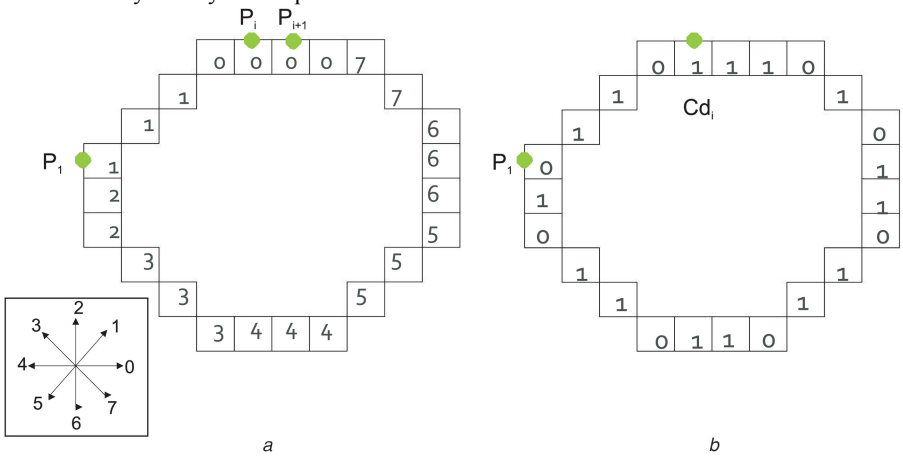

a *b*

Fig. 4 *Contour coding*
(a) Chain coding of shape boundary and directional codes (0–7), ***(b)*** Direction coding CD_i of each contour point P_i

shape 17 with respect to the secondary axis ($SP_s = 0.759$). This last value appears as a mismatch with respect to the previous observation of areas, but it can be explained by the fact that the contour is very irregular in the upper middle of the shape. Although in this case the contour follows the irregularity of the diatom, a similar situation could occur if the segmentation presents a high level of noise. A cross comparison between symmetry with respect to main or secondary axes shows that shape 6 has distinctive values in the corresponding descriptors (low SP_m, high SP_s).

Finally, shape 13 is the most radially symmetric (high mean, low standard deviation) in concordance with a visual appreciation. Notice that shape 2 is rounded and slightly elongated, which is exposed in the difference between values of $\mathrm{Min_A}$ and $\mathrm{Max_A}$. Shapes 4, 8, 7, and 15 are clearly non-symmetric radially and which is in concordance with the results on the table (low mean, high standard deviation). However, statistical descriptors for shape 5 could generate a false positive if we classify that shape as symmetric without taking into account the previous descriptors.

Table 1 Radial symmetry shape descriptors and their analytical definition

Radial symmetry shape descriptors	Symbol	Math definition
mean area	μ_{A}	$\frac{1}{6}\sum_{i=1,j=i+1}^{3} SA_{i,j}$
standard deviation of area	σ_{A}	$\sqrt{\frac{1}{5}\sum_{i=1,j=i+1}^{3}(SA_{i,j}-\mu_{\mathrm{A}})^2}$
maximum area	$\mathrm{Max_A}$	$\max(SA_{i,j})$
minimum area	$\mathrm{Min_A}$	$\min(SA_{i,j})$
mean perimeter	μ_{P}	$\frac{1}{6}\sum_{i=1,j=i+1}^{3} SP_{i,j}$
standard deviation of perimeter	σ_{P}	$\sqrt{\frac{1}{5}\sum_{i=1,j=i+1}^{3}(SP_i-\mu_{\mathrm{P}})^2}$
maximum perimeter	$\mathrm{Max_P}$	$\max(SP_{i,j})$
minimum perimeter	$\mathrm{Min_P}$	$\min(SP_{i,j})$

3.3 Shape classification with symmetry descriptors

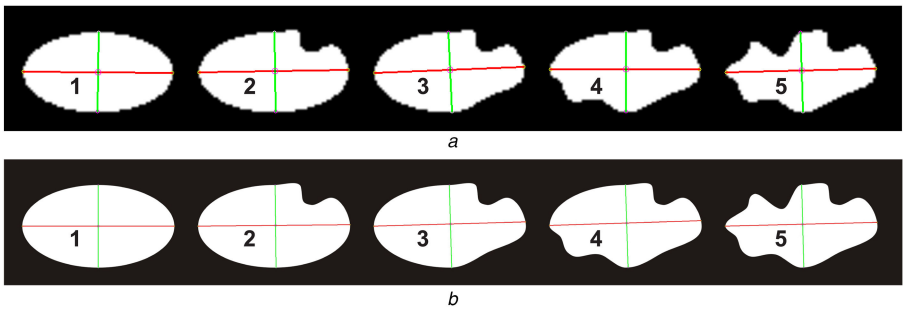

Fig. 6 *Set of shapes used to evaluate the descriptors*
(a) Image resolution: 400 × 233, ***(b)*** Image resolution: 1600 × 938

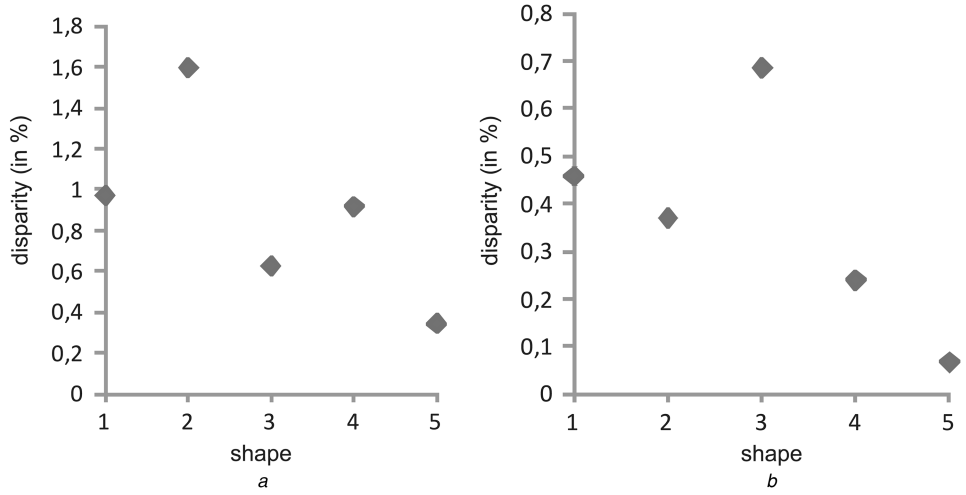

Fig. 7 *Disparity among the estimated and the actual main axis lengths*
(a) Low resolution image (Fig. 6*a*), ***(b)*** High resolution image (Fig. 6*b*)

We have evaluated the full set of all proposed descriptors in an object recognition test with 120 images extracted from MPGE-7 dataset (http://www.dabi.temple.edu/ shape/MPEG7/dataset.html). Several rotated and scaled versions of these images were built until forming a complete set of 840 shapes corresponding to six different classes. The considered classes were (face, spoon, device 7, bottle, watch, and break). The implementation details are shown in Algorithm 1.

To estimate the performance of the object recognition we used a 100-fold cross validation. The performance and confusion matrix are shown in Table 4. The diagonal values of the confusion matrix represent the percentage of correct prediction by the classifier, accounting for an average accuracy of 88% with a standard deviation of 1.06%.

Algorithm 1: Classification algorithm

1: FEATURE VECTOR:
2: for each shape S_i, $i \leftarrow 1, \ldots, N$, where N is the number of shapes in the dataset do
3: Extract contour C_i
4: Calculate the symmetry descriptors d_j, $j \leftarrow 1, \ldots, M$, with M to include all the proposed descriptors.
5: Create the feature vector $F_i \leftarrow (d_1 \times w_1, \ldots, d_j \times w_j, \ldots, d_M \times w_M)$, where $0 <= w_j <= 1$, $j = 1, \ldots, M$ is a weigh for each descriptor. $w_j \leftarrow 0$ means not considered.

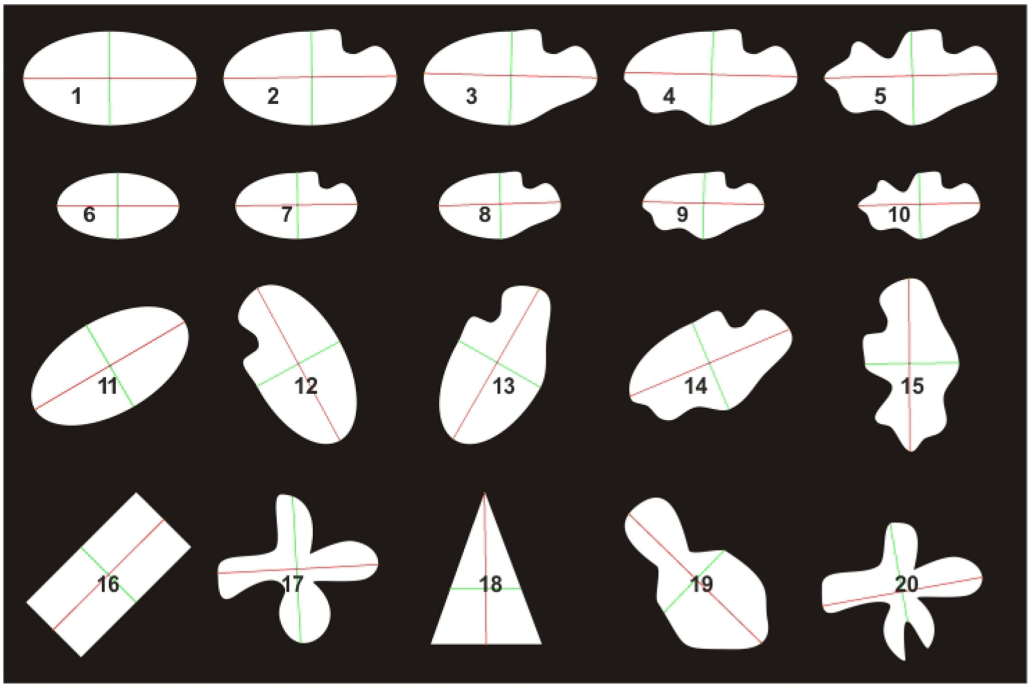

Fig. 8 *Synthetic images of various shapes used to evaluate the symmetry descriptors. In the first row, the shapes are the same as in Fig. 8. The second (resp. third) row are scaled (resp. rotated) versions thereof. The fourth row includes other special cases*

Table 2 Bilateral and radial symmetry shape descriptors from Fig. 8

Shape number	SA_m	SA_s	SP_m	SP_s	μ_A	σ_A	Max_A	Min_A	μ_P	σ_P	Max_P	Min_P
1	0.995	0.998	0.998	0.996	0.995	0.003	0.999	0.99	0.997	0.002	0.999	0.995
2	0.902	0.918	0.948	0.938	0.908	0.071	0.987	0.821	0.935	0.061	0.99	0.875
3	0.9	0.863	0.939	0.952	0.873	0.085	0.951	0.782	0.91	0.069	0.985	0.84
4	0.924	0.92	0.958	0.981	0.918	0.046	0.992	0.847	0.91	0.044	0.975	0.849
5	0.828	0.92	0.952	0.884	0.863	0.113	1	0.735	0.901	0.083	0.957	0.842
6	0.993	0.997	0.999	0.994	0.992	0.004	0.998	0.985	0.996	0.003	0.999	0.993
7	0.896	0.921	0.946	0.939	0.905	0.066	0.979	0.816	0.933	0.059	0.993	0.873
8	0.898	0.852	0.938	0.955	0.864	0.06	0.951	0.769	0.934	0.053	0.988	0.874
9	0.918	0.924	0.952	0.981	0.924	0.043	0.988	0.853	0.906	0.043	0.968	0.841
10	0.831	0.913	0.96	0.883	0.861	0.121	1	0.73	0.904	0.089	0.967	0.847
11	0.983	0.993	0.999	0.993	0.988	0.004	0.993	0.982	0.994	0.003	1	0.988
12	0.962	0.948	0.922	0.932	0.947	0.046	1	0.896	0.904	0.056	0.999	0.855
13	0.882	0.831	0.972	0.943	0.841	0.069	0.935	0.735	0.917	0.055	0.969	0.853
14	0.951	0.968	0.943	0.959	0.962	0.028	0.998	0.926	0.905	0.041	0.982	0.835
15	0.827	0.926	0.883	0.952	0.847	0.126	1	0.698	0.895	0.091	0.972	0.84
16	0.995	0.992	0.999	0.999	0.993	0.004	1	0.987	0.999	0.003	0.999	0.998
17	0.975	0.88	0.904	0.98	0.916	0.066	1	0.836	0.903	0.057	0.966	0.845
18	0.988	0.669	0.986	0.924	0.829	0.18	1	0.658	0.957	0.124	1	0.912
19	0.999	0.688	0.904	0.98	0.793	0.151	1	0.61	0.914	0.114	0.988	0.834
20	0.617	0.915	0.978	0.799	0.713	0.155	0.949	0.554	0.85	0.125	1	0.714

6: end for
7: DATA SPLIT:
8: Select n_p randomly prototypes representative of each class P_{hk}, $h \leftarrow 1, \ldots, n_p$, $k \leftarrow 1, \ldots, K$ (number of classes in the dataset).
9: CLASSIFICATION:
10: for each shape S_i which is not a prototype
11: Calculate the distance measure from F_i to each prototype $\text{dist}_{ihk} \leftarrow \| F_i - P_{hk} \|$
12: Choice de minimum dist_{ihk}, with $h \leftarrow 1, \ldots, n_p, k \leftarrow 1, \ldots, K$.
13: Assign the class K to the shape S_i.
14: end for

4 Conclusions and further work

Shape descriptors are useful for classification and recognition in computer vision. This paper provides the definition of a set of descriptors to evaluate the symmetry of objects. The descriptors are defined in terms of the relation of areas and perimeters based on the subdivision of a shape through a main axis and a secondary axis. The axes are obtained after a correction stage applied to the main axis length.

The proposed symmetry descriptors were applied both to synthetic and real images. With synthetic images two different shape sets were considered. In the first case, the axes estimation was evaluated for low and high resolution images, arriving to the conclusion that the correction level of the main axis is inversely proportional to the image resolution. The second case aimed to evaluate the sensitivity to changes in orientation and scaling. Even though the shape descriptors are purely based on affine operations, the invariance under affine transformations in discrete imagery

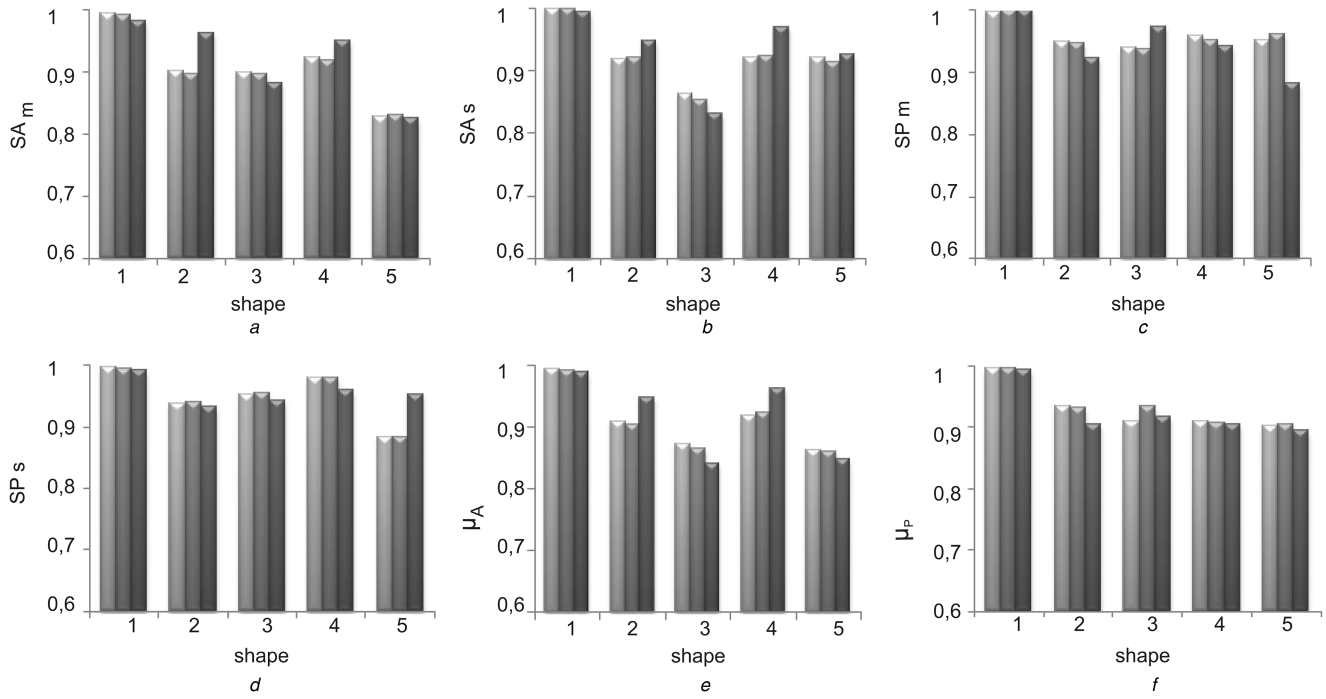

Fig. 9 *Bilateral and radial symmetry descriptors based on area and perimeter for each shape proposed in Fig. 8*
(a) Bilateral symmetry of the main axis based on area, ***(b)*** Bilateral symmetry of the secondary axis based on area, ***(c)*** Bilateral symmetry of the main axis based on perimeter, ***(d)*** Bilateral symmetry of the secondary axis based on perimeter, ***(e)*** Mean of radial symmetry based on area, ***(f)*** Mean of radial symmetry based on perimeter

depends on the coarseness of the discretisation, and therefore scale invariance may be affected in small scales.

In the analysis of the shape descriptors in real images, a set of diatom images was used, including with a variety of samples to analyse. In these images, it was possible to identify the most and least symmetric shapes, in some cases using only one symmetry axis, and in other cases using both. The results basically match the human perception of symmetry in these shapes. In addition, we showed the usefulness of a statistical evaluation of the descriptors in some particular shapes.

These preliminary results show that the proposed symmetry-based shape descriptors are useful in assessing symmetry properties in a way 'that appears to be' similar to the human eye. A simple object recognition test was performed and obtained results showed that the proposed symmetry descriptors are adequate for classification purposes. An even finer assessment may be achieved using more sophisticated techniques like multivariate analysis, canonical correlation analysis, or PCA.

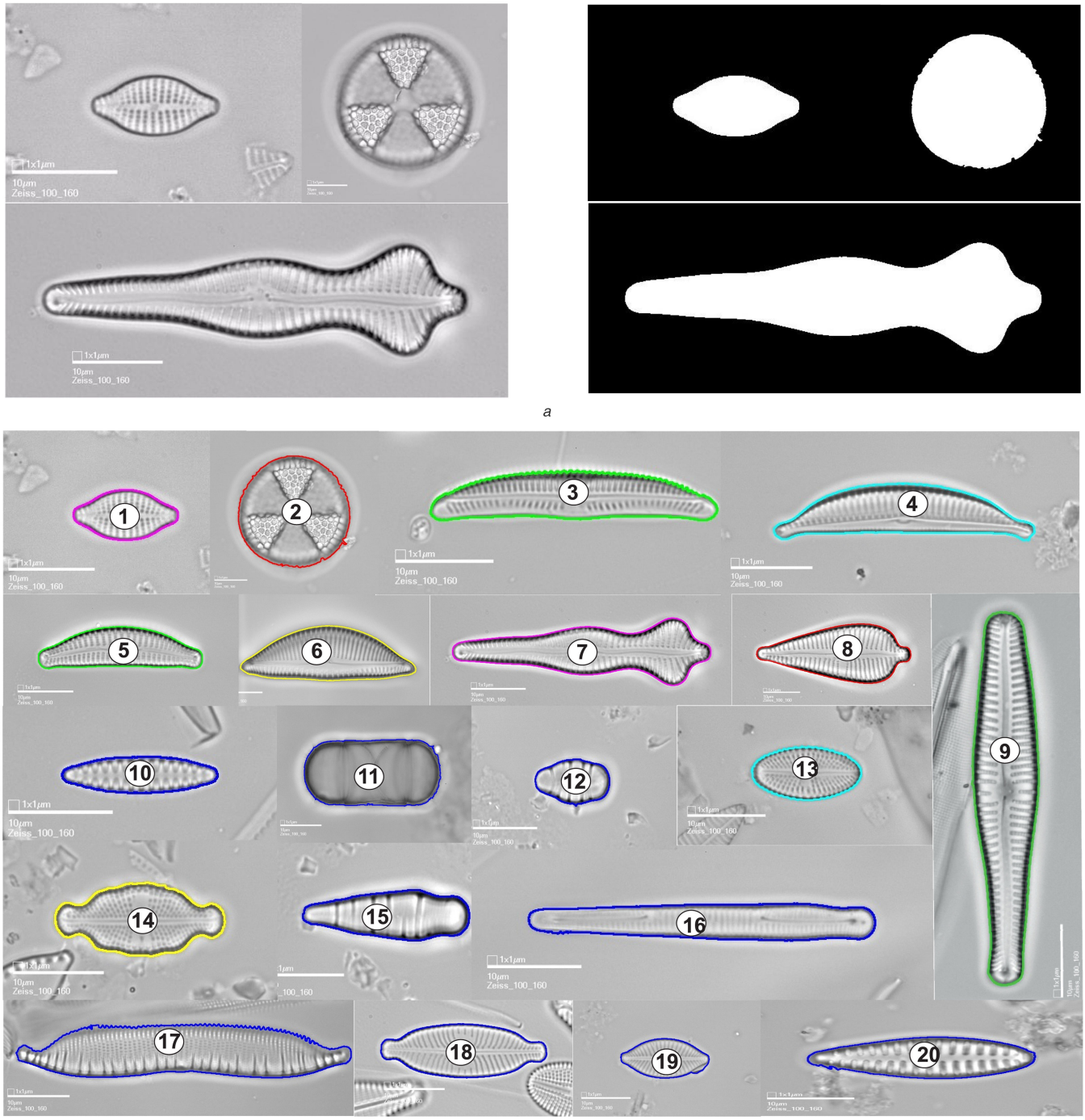

Fig. 10 *Set of diatoms used to evaluate the descriptors*

(a) Three examples of diatoms in a grey level image (left). Segmented images into a binary image for the three examples of diatoms (right), ***(b)*** Different diatoms bilaterally symmetrical about two orthogonal axes, bilaterally symmetrical about only one axis and rotational symmetrical

Table 3 Bilateral and radial symmetry shape descriptors from Fig. 10*b*

Shape number	SA_m	SA_s	SP_m	SP_s	μ_A	σ_A	Max_A	Min_A	μ_P	σ_P	Max_P	Min_P
1	0.93	0.971	0.989	0.989	0.93	0.037	0.975	0.888	0.987	0.026	0.999	0.975
2	0.998	0.881	0.99	0.943	0.926	0.053	0.997	0.888	0.969	0.04	1	0.935
3	0.934	0.988	0.882	0.985	0.846	0.086	0.97	0.747	0.877	0.073	0.966	0.803
4	0.815	0.961	0.783	0.994	0.754	0.135	0.878	0.557	0.765	0.131	0.991	0.615
5	0.98	0.998	0.907	0.986	0.982	0.01	0.997	0.965	0.919	0.02	0.968	0.889
6	0.9654	0.998	0.838	0.997	0.884	0.059	0.957	0.797	0.834	0.067	0.943	0.743
7	0.998	0.705	0.917	0.99	0.789	0.141	1	0.661	0.943	0.099	1	0.904
8	0.991	0.705	0.975	0.981	0.799	0.154	1	0.693	0.982	0.104	1	0.957
9	0.972	0.788	0.989	0.975	0.816	0.088	0.912	0.679	0.973	0.061	0.995	0.948
10	0.894	0.985	0.966	0.991	0.906	0.052	0.994	0.863	0.967	0.037	0.992	0.949
11	0.991	0.981	0.99	0.986	0.891	0.063	0.978	0.826	0.921	0.055	0.995	0.877
12	0.952	0.913	0.972	0.989	0.939	0.032	0.975	0.881	0.974	0.023	0.989	0.957
13	0.985	0.974	0.966	0.991	0.948	0.028	0.987	0.916	0.973	0.025	0.999	0.934
14	0.972	0.979	0.989	0.989	0.954	0.032	0.994	0.916	0.975	0.024	0.997	0.956
15	0.981	0.777	0.978	0.992	0.83	0.111	1	0.69	0.983	0.075	0.999	0.957
16	0.933	0.797	0.996	0.971	0.83	0.097	0.965	0.707	0.968	0.067	0.994	0.938
17	0.779	0.959	0.962	0.759	0.843	0.069	0.947	0.734	0.827	0.086	0.991	0.729
18	0.955	0.988	0.995	0.998	0.922	0.04	0.962	0.873	0.979	0.028	0.997	0.968
19	0.974	0.95	0.968	0.993	0.917	0.041	0.974	0.861	0.952	0.032	0.974	0.914
20	0.977	0.801	0.98	0.957	0.859	0.089	1	0.77	0.957	0.063	0.999	0.916

Table 4 Classification performance

(a) Matrix confusion matrix

			Predicted			
	face	*spoon*	*device7*	*bottle*	*watch*	*break*
Actual						
face	96%	0	4%	0	0	0
spoon	0	90%	0	8%	2%	0
device7	7%	0	84%	0	4%	5%
bottle	0	6%	0	89%	5%	0
watch	6%	0	4%	5	80%	5%
break	0	0	5%	0	2%	93%

(b) Accuracy classification precision, sensitivity, and specificity

	Precision	Sensitivity	Specificity
Class			
face	0.88	0.96	0.97
spoon	0.93	0.90	0.98
device7	0.86	0.84	0.97
bottle	0.87	0.84	0.97
watch	0.86	0.80	0.97
break	0.90	0.93	0.98

5 References

[1] Neal, F.B., Russ, J.C.: '*Measuring shape*' (CRC Press, Boca Raton, 2012)

[2] Sluzek, A.: 'Identification and inspection of 2-d objects using new moment-based shape descriptors', *Pattern Recognit. Lett.*, 1995, **16**, (7), pp. 687–697. doi: http://dx.doi.org/10.1016/0167-8655(95)00021-8. URL http://www.sciencedirect.com/science/article/pii/0167865595000218

[3] Sparks, R., Madabhushi, A.: 'Explicit shape descriptors: novel morphologic features for histopathology classification', *Med. Image Anal.*, 2013, **17**, (8), pp. 997–1009. doi: http://dx.doi.org/10.1016/j.media.2013.06.002. URL http://www.sciencedirect.com/science/article/pii/S136184151300087X

[4] Zandonadi, R., Luck, J., Stombaugh, T., *et al.*: 'Evaluating field shape descriptors for estimating off-target application area in agricultural fields', *Comput. Electron. Agric.*, 2013, **96**, (0), pp. 217–226. doi: http://dx.doi.org/10.1016/j.compag.2013.05.011. URL http://www.sciencedirect.com/science/article/pii/S0168169913001312

[5] Xue, M., Xu, L., Zhou, G.: 'A new shape descriptor for object recognition'. Int. Conf. on Electrical and Control Engineering (ICECE), 2011, 2011, pp. 5673–5676. doi: 10.1109/ICECENG.2011.6057080

[6] Patki, A., Patterson, E.: 'Decomposing strain maps using Fourier-Zernike shape descriptors', *Exp. Mech.*, 2012, **52**, (8), pp. 1137–1149. doi: 10.1007/s11340-011-9570-4. URL http://dx.doi.org/10.1007/s11340-011-9570-4

[7] Zhang, D., Lu, G.: 'Review of shape representation and description techniques', *Pattern Recogn.*, 2004, **37**, (1), pp. 1–19. doi: http://dx.doi.org/10.1016/j.patcog.2003.07.008. URL http://www.sciencedirect.com/science/article/pii/S0031320303002759

[8] Shi, Y., Wang, G., Wang, R., *et al.*: 'Contour descriptor based on space symmetry and its matching technique', *Optik – Int. J. Light Electron Opt.*, 2013, **124**, (23), pp. 6149–6153. doi: http://dx.doi.org/10.1016/j.ijleo.2013.04.132. URL http://www.sciencedirect.com/science/article/pii/S0030402613007298

[9] Peura, M., Iivarinen, J.: 'Efficiency of simple shape descriptors'. Aspects of Visual Form, 1997, pp. 443–451

[10] Rauber, T.W., Steiger-Garão, A.S.: '2-d form descriptors based on a normalized parametric polar transform (unl transform)'. MVA, 1992

[11] Rui, Y., She, A.C., Huang, T.S.: 'A modified Fourier descriptor for shape matching in mars', MARS, in Chang, S.K. (ED.) '*Image databases and multimedia search, series of software engineering and knowledge engineering*' (World Scientific Publishing, 1998), pp. 165–180

[12] Belongie, S., Malik, J., Puzicha, J.: 'Shape matching and object recognition using shape contexts', *IEEE Trans. Pattern Anal. Mach. Intell.*, 2001, **24**, pp. 509–522

[13] Chai, L., Qin, Z., Li, Q., *et al.*: 'Ordered histogram of shapemes: an ordered bag-of-features based shape descriptor for efficient shape matching'. IEEE Int. Conf. on Image Processing (ICIP)

[14] Rauber, T.W., Steiger-Garcao, A.S.: 'Shape description by unl Fourier features an application to handwritten character recognition'. Proc., 11th IAPR Int. Conf. on Pattern Recognition, 1992. Vol. II. Conf. B: Pattern Recognition Methodology and Systems, 1992, pp. 466–469. doi: 10.1109/ICPR.1992.201819

[15] Dudek, G., Tsotsos, J.K.: 'Shape representation and recognition from multiscale curvature', *Comput. Vis. Image Underst.*, 1997, **68**, (2), pp. 170–

189. doi: http://dx.doi.org/10.1006/cviu.1997.0533. URL http://www.sciencedirect.com/science/article/pii/S1077314297905336
[16] Freeman, H.: 'On the encoding of arbitrary geometric configurations', *IRE Trans. Electron. Comput.*, 1961, **EC-10**, (2), pp. 260–268. doi: 10.1109/TEC.1961.5219197
[17] Alexander, K., Pasi, F.: '*Polygonal approximation of closed contours*' (Springer Berlin Heidelberg, Berlin, Heidelberg, 2003), pp. 778–785. doi: 10.1007/3-540-45103-X-103
[18] Jain, R., Kasturi, R., Schunck, B.G.: '*Machine vision*' (McGraw-Hill, 1995)
[19] Bimbo, A.D., Pala, P.: 'Visual image retrieval by elastic matching of user sketches', *IEEE Trans. Pattern Anal. Mach. Intell.*, 1997, **19**, (2), pp. 121–132. doi: 10.1109/34.574790
[20] Flusser, J., Suk, T.: 'Pattern recognition by affine moment invariants', *Pattern Recogn.*, 1993, **26**, (1), pp. 167–174. doi: http://dx.doi.org/10.1016/0031-3203(93)90098-H. URL http://www.sciencedirect.com/science/article/pii/003132039390098H
[21] Huang, Z., Cohen, F.S.: 'Affine-invariant b-spline moments for curve matching'. 1994 IEEE Computer Society Conf. on Computer Vision and Pattern Recognition, 1994, Proc. CVPR '94, 1994, pp. 490–495. doi: 10.1109/CVPR.1994.323871
[22] Kan, C., Srinath, M.D.: 'Invariant character recognition with Zernike and orthogonal Fourier–Mellin moments', *Pattern Recogn.*, 2002, **35**, (1), pp. 143–154, shape representation and similarity for image databases. doi: http://dx.doi.org/10.1016/S0031-3203(00)00179-5. URL http://www.sciencedirect.com/science/article/pii/S0031320300001795
[23] Zhang, H., Shu, H., Haigron, P.*, et al.*: 'Construction of a complete set of orthogonal Fourier Mellin moment invariants for pattern recognition applications', *Image Vis. Comput.*, 2010, **28**, (1), pp. 38–44. doi: http://dx.doi.org/10.1016/j.imavis.2009.04.004. URL http://www.sciencedirect.com/science/article/pii/S0262885609000730
[24] Farajzadeh, N., Faez, K., Pan, G.: 'Study on the performance of moments as invariant descriptors for practical face recognition systems', *IET Comput. Vis.*, 2010, **4**, pp. 272–285(13). URL http://digital-library.theiet.org/content/journals/10.1049/iet-cvi.2009.0140
[25] Wei, W., Yongmei, J., Lingjun, Z.*, et al.*: 'Contour matching using the affine-invariant support point set', *IET Comput. Vis.*, 2014, **8**, pp. 35–44(9). URL http://digital-library.theiet.org/content/journals/10.1049/iet-cvi.2013.0031
[26] Klette, R., Uni, J.: '*f*ADRg shape descriptor distance between shape centroids versus shape diameter', *Comput. Vis. Image Underst.*, 2012, **116**, (6), pp. 690–697. doi: http://dx.doi.org/10.1016/j.cviu.2012.02.001. URL http://www.sciencedirect.com/science/article/pii/S1077314212000331
[27] Ban, H., Yamamoto, H., Fukunaga, M.*, et al.*: 'Toward a common circle: interhemispheric contextual modulation in human early visual areas', *J. Neurosci.*, 2006, **26**, (34), pp. 8804–8809. arXiv: http://www.jneurosci.org/content/26/34/8804.full.pdf+html, doi: 10.1523/JNEUROSCI.1765-06.2006. URL http://www.jneurosci.org/content/26/34/8804.abstract
[28] Dakin, S., Herbert, A.: 'The spatial region of integration for visual symmetry detection', *Proc. R. Soc. Lond. B, Biol. Sci.*, 1998, **265**, (1397), pp. 659–664. arXiv: http://rspb.royalsocietypublishing.org/content/265/1397/659.full.pdf+html, doi: 10.1098/rspb.1998.0344. URL http://rspb.royalsocietypublishing.org/content/265/1397/659.abstract
[29] Beck, D.M., Pinsk, M.A., Kastner, S.: 'Symmetry perception in humans and macaques', *Trends Cogn. Sci.*, 2005, **9**, (9), pp. 405–406. doi: http://dx.doi.org/10.1016/j.tics.2005.07.002. URL http://www.sciencedirect.com/science/article/pii/S1364661305002068
[30] Feng, Q., Zhang, X.: 'Visual inspection for circular objects based on global symmetry', *fAASRIg Proc.*, 2012, **3**, (0), pp. 559–565, Conf. on Modelling, Identification and Control. doi: http://dx.doi.org/10.1016/j.aasri.2012.11.088. URL http://www.sciencedirect.com/science/article/pii/S2212671612002478
[31] Pfeifer, R., Bongard, J.C.: '*How the body shapes the way we think: a new view of intelligence (Bradford Books)*' (The MIT Press, 2006)
[32] Farrera, A., Villanueva, M., Quinto-Sánchez, M.*, et al.*: 'The relationship between facial shape asymmetry and attractiveness in Mexican students', *Am. J. Hum. Biol.*, 2015, **1**, (1), pp. 1–8
[33] Parui, S., Majumder, D.D.: 'Symmetry analysis by computer', *Pattern Recogn.*, 1983, **16**, (1), pp. 63–67. doi: http://dx.doi.org/10.1016/0031-3203(83)90009-2. URL http://www.sciencedirect.com/science/article/pii/0031320383900092
[34] Loy, G., Eklundh, J.-O.: '*Detecting symmetry and symmetric constellations of features*' (Springer Berlin Heidelberg, Berlin, Heidelberg, 2006), pp. 508–521
[35] Schmitt, O., Hasse, M.: 'Radial symmetries based decomposition of cell clusters in binary and gray level images', *Pattern Recogn.*, 2008, **41**, (6), pp. 1905–1923. doi: http://dx.doi.org/10.1016/j.patcog.2007.11.006. URL http://www.sciencedirect.com/science/article/pii/S0031320307004967
[36] Otsu, N.: 'A threshold selection method from gray-level histograms', *IEEE Trans. Syst. Man Cybern.*, 1979, **9**, (1), pp. 62–66. doi: 10.1109/tsmc.1979.4310076. URL http://dx.doi.org/10.1109/tsmc.1979.4310076